The Causes and Consequences of Phase Unbalance in Single-Sided Linear Induction Motors

K. ADAMIAK, KRISHNAMOORTHY ANANTHASIVAM, GRAHAM E. DAWSON, MEMBER, IEEE, ANTHONY R. EASTHAM, SENIOR MEMBER, IEEE, AND JACEK F. GIERAS, MEMBER, IEEE

Abstract—**Unbalance in the phase currents of a single-sided linear induction motor (LIM) under balanced voltage operation is due to asymmetry of the primary windings and to the longitudinal end effect. In this paper, two methods of evaluating phase unbalance are presented. The first, analytical, is based on an equivalent circuit model. The second approach, numerical, uses the finite-element method. Computational results are validated by comparison with test results on a large-scale single-sided LIM at Queen's University. It is shown that phase unbalance produces a reduction in both thrust and normal forces, but this effect is likely to be significant only for high-speed LIM's.**

I. INTRODUCTION

THERE IS A WEALTH of literature on the analysis of linear induction motors (LIM's). The nature of the primary winding configuration, excitation, and reaction rail geometry of useful machines requires certain simplifying assumptions to be made for analysis to be tractible. It has been common to use the assumptions of balanced sinusoidal time and space variations, i.e., sinusoidal excitation and a sinusoidally distributed primary current sheet, producing a forward-traveling magnetic-flux density wave in the airgap of the machine. Analysis may then proceed to the solution of the two- (2D) or three-dimensional (3D) electromagnetic field distribution by using a multi-layer model of the machine, by a space-harmonic (Fourier analysis or transform) technique, or by finite-difference or finite-element techniques.

The phase unbalance characteristics of LIM's have attracted some interest in the literature [1]–[8]. Under balanced terminal voltage conditions, the current unbalance in a LIM of finite length is due to asymmetry of the phase windings and to the longitudinal end effect. Under standstill conditions, the longitudinal end effect is nonexistent and any unbalance in phase currents is caused by the asymmetric distribution of phase windings along the length of the machine. This unbalance is typically 1–2 percent, and its effect is small compared to that under dynamic conditions. The longitudinal end effect produces a velocity-dependent nonuniformity of the airgap flux distribution along the length of the machine. Consequently, the total impedance of each phase of a LIM is unequal; i.e., $Z_A \neq Z_B \neq Z_C$.

It is convenient to use the method of symmetrical components [9], [10] to evaluate the phase currents resulting from balanced voltages and unbalanced phase impedances, and to evaluate LIM performance from the resultant positive and negative sequence fields. Most authors have found that LIM performance is rather insensitive to small phase unbalance. Sankaran *et al.* [2] found that an unbalance factor (negative/positive sequence component) of about 0.2 was required to degrade thrust significantly. Substantial unbalance and thrust degradation was observed by Bolopion *et al.* [7] in their two-pole gramme wound motor.

In this paper, we present analyses for evaluating the thrust and normal forces of a LIM including phase unbalance and, by validation with test results from a large-scale six-pole LIM, we show that the analyses can be applied to machines designed as transportation drives.

II. ANALYTICAL APPROACH

A. Formulation of the Problem

The MMF of each phase of a three-phase machine with primary windings displaced by the space angle $2\pi/3$ and fed with unbalanced currents can be expressed by the following set of equations:

$$F_A(x,t) = \frac{2}{\pi}\frac{1}{p} Nk_w \cos\left(\frac{\pi}{\tau}x - 0\frac{2\pi}{3}\right)\sqrt{2}\,|I_A|\,e^{j(\omega t-\beta_A)}$$

$$F_B(x,t) = \frac{2}{\pi}\frac{1}{p} Nk_w \cos\left(\frac{\pi}{\tau}x - 1\frac{2\pi}{3}\right)\sqrt{2}\,|I_B|\,e^{j(\omega t-\beta_B)}$$

$$F_C(x,t) = \frac{2}{\pi}\frac{1}{p} Nk_w \cos\left(\frac{\pi}{\tau}x - 2\frac{2\pi}{3}\right)\sqrt{2}\,|I_C|\,e^{j(\omega t-\beta_C)} \quad (1)$$

where β_A, β_B, and β_C are the phase angles between currents. Subsequently, we set $\beta_A = 0$.

Manuscript received May 7, 1987; revised June 2, 1988. This work was supported by the Transportation Development Centre of Transport Canada and by the Natural Sciences and Engineering Research Council (NSERC) of Canada. The work of J. F. G. (for the year 1983–1984) and K. A. (for the year 1986–1987) was supported by NSERC under International Scientific Exchange Awards to conduct research at Queen's University.

K. Adamiak is with the Department of Electrical Engineering, Queen's University, Kingston, Ont., Canada K7L 3N6, on leave from the Kielce University of Technology, Kielce, Poland.

K. Ananthasivam, G. E. Dawson, and A. R. Eastham are with the Department of Electrical Engineering, Queen's University, Kingston, Ont., Canada K7L 3N6.

J. F. Gieras was with the Department of Electrical Engineering, Queen's University, Kingston, Ont., Canada K7L 3N6. He is now with the Academy of Technology and Agriculture, Bydgoszcz, Poland.

IEEE Log Number 8823362.

Denoting

$$I^+ = \tfrac{1}{3}(I_A + aI_B + a^2 I_C) \tag{2a}$$

$$I^- = \tfrac{1}{3}(I_A + a^2 I_B + aI_C) \tag{2b}$$

where

$$I_A = |I_A| \exp(-j\beta_A)$$
$$I_B = |I_B| \exp(-j\beta_B)$$
$$I_C = |I_C| \exp(-j\beta_C)$$

and

$$a = \exp(j2\pi/3)$$

the total MMF of a three-phase machine can be expressed as

$$F(x, t) = F_A(x, t) + F_B(x, t) + F_C(x, t) = \frac{3\sqrt{2}Nk_w}{\pi p}\left[I^+ e^{j[\omega t - (\pi/\tau)x]} + I^- e^{j[\omega t + (\pi/\tau)x]}\right]. \tag{3}$$

Equation (3) describes two MMF waves traveling in opposite directions, with the coordinate system fixed to the primary. Differentiating with respect to x and putting $\beta = \pi/\tau$, (3) yields the line-current density of the primary [20]

$$a(x, t) = \frac{d[F(x, t)]}{dx} = A_m^+ e^{j[\omega t - \beta x - (\pi/2)]} + A_m^- e^{j[\omega t + \beta x + (\pi/2)]} \tag{4}$$

where

$$A_m^+ = \frac{3\sqrt{2}|I^+|Nk_w}{\tau p} \tag{5a}$$

$$A_m^- = \frac{3\sqrt{2}|I^-|Nk_w}{\tau p}. \tag{5b}$$

Equation (4), together with Maxwell's equations and the boundary conditions, gives the two-dimensional (2D) electromagnetic field distribution in the airgap and in the secondary.

From (2a) and (2b) it is seen that, for $|I_A| = |I_B| = |I_C|$ and $\beta_A = 0$, $\beta_B = 120°$, $\beta_C = 240°$, the MMF in phases A, B, and C constitutes a symmetrical three-ray star with positive sequence only ($I^+ \neq 0$; $I^- = 0$). For $|I_A| \neq |I_B| \neq |I_C|$ and $\beta_A = 0$, $\beta_B \neq 120°$, and $\beta_C \neq 240°$, phase currents produce both positive-sequence and negative-sequence line-current densities in the primary.

B. Equivalent Circuit with Phase Unbalance

The analysis of LIM performance under constant voltage conditions can be performed conveniently with the T-type equivalent circuit. This method, including skin effect in the secondary, saturation, hysteresis, and transverse edge effect has been described in detail [11], [12]. We also have reported success in taking into account the longitudinal end effect by introducing an end-effect factor [13]. The present paper develops this last idea by formulating different end factors for each phase. Asymetry of phase winding impedances due to finite length of the magnetic circuit is considered to be a minor effect (confirmed by the very small unbalance of the test LIM at standstill) and is not taken into account.

The magnetic field in the airgap of a LIM may be considered as the superposition of two traveling waves [14]

$$b(x, t) = b_s(x, t) + b_e(x, t) \tag{6}$$

where

$$b_s(x, t) = B_{ms} \sin\left(\omega t - \frac{\pi}{\tau}x\right)$$

$$b_e(x, t) = B_{me} e^{-x/T_e} \sin\left(\omega t - \frac{\pi}{\tau_e}x + \delta\right).$$

Both waves induce a voltage in the primary winding

$$e(t) = e_s(t) + e_e(t) = -E_{ms} \cos \omega t + E_{me} \cos \omega t. \tag{7}$$

The end-effect factor is defined by the equation

$$k_e = \frac{E_{me}}{E_{ms}}. \tag{8}$$

The instantaneous values of both components in (7) can be calculated by taking the time derivative of the magnetic flux linkage [13]

$$e_s(t) = -pN_p k_w L \frac{d}{dt}\int_0^\tau B_{ms} \sin\frac{\pi}{\tau}x\, dx \sin \omega t \tag{9a}$$

$$e_e(t) = -\sum_{k=1}^{p} N_{pe} k_{we} \frac{d}{dt}\phi_{e2k-1}. \tag{9b}$$

Equations (9a) and (9b) do not allow for differences between phases, and phase unbalance cannot be taken into account. To achieve this, the flux linkage must be calculated separately for each phase. For the first pole

$$\phi_{1A}^{\text{new}} = \phi_{1A}$$
$$\phi_{1C}^{\text{new}} = \phi_{1C} - \phi'_{1C} \tag{10a}$$

where

$$\phi'_{1C}(t) = LB_{me} \sin \omega t \int_0^{\tau/3} e^{-x/T_e} \sin\left(\frac{\pi}{\tau_e}x + \delta\right) dx$$

$$\phi_{1B}^{\text{new}} = \phi_{1B} - \phi'_{1B} \tag{10b}$$

where

$$\phi'_{1B}(t) = LB_{me} \sin \omega t \int_0^{2\tau/3} e^{-x/T_e} \sin\left(\frac{\pi}{\tau_e}x + \delta\right) dx. \tag{10c}$$

Considering the differences in space position of each phase more strictly, a similar correction should also be

performed for the last pole flux. However, the end-effect wave is attenuated very rapidly at the back of the LIM, and this correction is insignificant.

Performing calculations according to (7)–(10), the longitudinal end-effect factors for each phase, k_{eA}, k_{eB}, and k_{eC}, can be obtained.

The equivalent circuit of one phase of a LIM, including end effect, is shown in Fig. 1(a). The end effect impedance Z_e is [13]

$$Z_e = \frac{1 - k_e}{k_e} Z_t \tag{11}$$

where total impedance of magnetizing and secondary branches Z_t is given by

$$Z_t = \frac{Z_g Z'_{\text{sec}}}{Z_g + Z'_{\text{sec}}}. \tag{12}$$

The terminal impedance of the single phase circuit shown in Fig. 1(a) is

$$Z = Z_p + \frac{Z_e Z_t}{Z_e + Z_t}. \tag{13}$$

Equation (13) can be rewritten

$$Z = Z_{pe} + Z_t \tag{14}$$

where

$$Z_{pe} = Z_p - k_e Z_t. \tag{15}$$

This implies that the difference in the equivalent circuit for each phase can be lumped into the primary impedance (15) by assuming symmetry in magnetizing and secondary branches (Fig. 1(b)). It is simpler to analyze the equivalent circuit of a LIM with unequal equivalent impedances of the primary winding than with an inequality in all circuit impedances [9], [10].

If the LIM is supplied from a symmetrical three-phase voltage source, the positive and negative sequence voltages can be written in complex form as

$$V^+ = \frac{1}{3}(V_A + aV_B + a^2V_c) = V \tag{16a}$$

$$V^- = \frac{1}{3}(V_A + a^2V_B + a\,V_c) = 0 \tag{16b}$$

where

$$V_A = |V|$$

$$V_B = |V| \exp\left(-j\frac{2\pi}{3}\right)$$

$$V_C = |V| \exp\left(-j\frac{4\pi}{3}\right).$$

With no neutral connection, there is no zero-sequence current, and positive and negative sequence currents may be calculated as (see the Appendix)

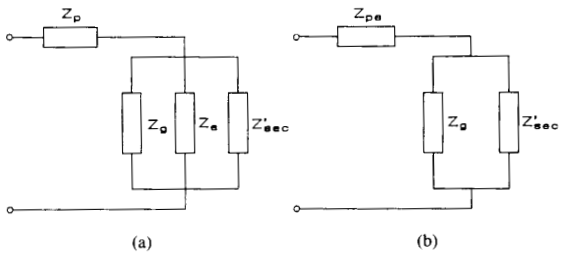

Fig. 1. Equivalent circuit of LIM with end effect taken into account with (a) parallel end-effect impedance Z_e and (b) equivalent stator winding impedance Z_{pe}.

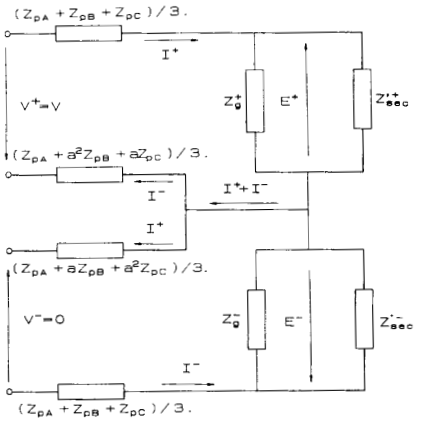

Fig. 2. Equivalent circuit of LIM including unbalance.

$$I^+ = \frac{3V^+}{Z_{p0} + 3Z_t^+ - \dfrac{Z_p^+ Z_p^-}{Z_{p0} + 3Z_t^-}} \tag{17a}$$

$$I^- = -I^+ \frac{Z_p^+}{Z_{p0} + 3Z_t} \tag{17b}$$

where

$$Z_{p0} = Z_{pA} + Z_{pB} + Z_{pC}$$

$$Z_p^+ = Z_{pA} + aZ_{pB} + a^2Z_{pC}$$

$$Z_p^- = Z_{pA} + a^2Z_{pB} + aZ_{pC}.$$

The equivalent circuit of a LIM including unbalance is shown in Fig. 2. The voltage equations establishing the equivalent circuit and currents I^+, I^- according to (17a) and (17b) are developed in the Appendix. Expressions for the secondary impedance Z'_{sec} and for the magnetizing branch impedance Z_g are given in [11], [15]

C. LIM Performance

The airgap EMF, the secondary current referred to the primary circuit, the electromagnetic power, and the electromagnetic thrust can be expressed as follows:

- for positive-sequence currents

$$E^+ = |I^+||Z_t^+| \tag{18a}$$

$$I'^+_{\text{sec}} = E^+/|Z'^+_{\text{sec}}| \tag{19a}$$

$$P^+_{em} = 3|I'^+_{\text{sec}}|^2 \operatorname{Re}[Z'^+_{\text{sec}}] \tag{20a}$$

$$F^+_x = P^+_{em}/v_s \tag{21a}$$

- for negative-sequence currents

$$E^- = |I^-||Z_t^-| \tag{18b}$$

$$I'^-_{\text{sec}} = E^-/|Z'^-_{\text{sec}}| \tag{19b}$$

$$P^-_{em} = 3|I'^-_{\text{sec}}|^2 \operatorname{Re}[Z'^-_{\text{sec}}] \tag{20b}$$

$$F^-_x = P^-_{em}/v_s. \tag{21b}$$

The total thrust is then

$$F_x = F^+_x + F^-_x. \tag{22}$$

The normal force is given by

$$F_z = \frac{A}{4\mu_0}\left[(B_{mz})^2 - \frac{B_{mx}}{B_{mz}}|F_x|\right] \tag{23}$$

where A is the active surface area of the LIM.

The power input, power output, efficiency, and power factor can also be readily calculated using the equivalent circuit.

III. Finite-Element Approach

The vector magnetic potential A in nonlinear, conducting, and moving media is governed by the equation

$$\nabla \times \nu\nabla \times A = -J_s + \sigma\left(-\frac{\partial A}{\partial t} + v \times \Delta \times A\right). \tag{24}$$

The conventional, complex steady-state, finite-element technique applied to the above equation gives the following matrix equation for unknown values of the vector magnetic potential at nodes of the mesh [16]:

$$\nu[S][A] + j\omega\sigma[T][A] + \sigma v[Q][A] = [T][J_s]. \tag{25}$$

This finite-element formulation allows the magnetic field to be calculated when the excitation current is given. In most practical situations, however, the excitation voltage is known, and the excitation currents depend on the circuit impedance, which is a function of field distribution. In such cases, modification of the finite-element method is necessary [17]–[19] in order that both the current and the vector potential can be evaluated.

The terminal voltages are related to the current through the winding impedance. The loop equation for each phase can be written as

$$-j\omega \int_c A\, dl + R_p I_p + jX_e I_p = V_p \tag{26}$$

TABLE I
Design Parameters of Test LIM

Primary:	
number of phases	3
number of pole pairs	3
pole pitch	0.25 m
width of primary stack	0.101 m
number of slots per pole per phase	3
coil pitch	0.1994 m
number of series turns/phase	108
nominal (mean) phase current	200 A
nominal airgap	15 mm
Secondary:	
width of solid steel core	0.111 mm
depth of solid steel core	25.4 mm
thickness of aluminum cap over core	4.5 mm
cross section of aluminum end bars	571.5 mm^2
conductivity of aluminum cap (at 20°C)	32.3 × 10^6 S/m

where

- c contour along the winding
- X_e end winding leakage reactance
- R_p primary resistance.

Equation (26), formulated for each phase, and (25) create the final matrix equation to solve the problem with known terminal voltage

$$\begin{matrix}[D][A] = [U]. \\ [J]\end{matrix} \tag{27}$$

The magnetic field distribution in a LIM has been calculated by means of the finite-element method making the following assumptions.

- The problem is two-dimensional (the field distribution is uniform in the z direction). Transverse edge effects are accounted for by correcting the secondary conductivity using the Russell and Norsworthy factor [20].
- Ferromagnetic materials are nonlinear and isotropic.
- Induced currents in the current-carrying conductors are neglected.

A longitudinal cross section of the test LIM has been discretized using triangular elements of first order. The matrix equation (27) with banded and nonsymmetric matrix $[D]$ was solved by means of the well-known Newton-Raphson technique.

The thrust and normal forces were evaluated using the Lorentz equation

$$F_x = \frac{w}{2}\iint JB^*_z\, ds \tag{28a}$$

$$F_z = -\frac{w}{2}\left[\iint JB^*_x\, ds + \frac{1}{2\mu}\int [B^2_z - B^2_x]\, dx\right]. \tag{28b}$$

IV. Results of Calculations and Experiments

Experiments have been performed for the linear induction motor tested on the Canadian Institute of Guided Ground Transport (CIGGT) facility at Queen's University [21]. This test facility uses a 7.6-m-diameter rotating

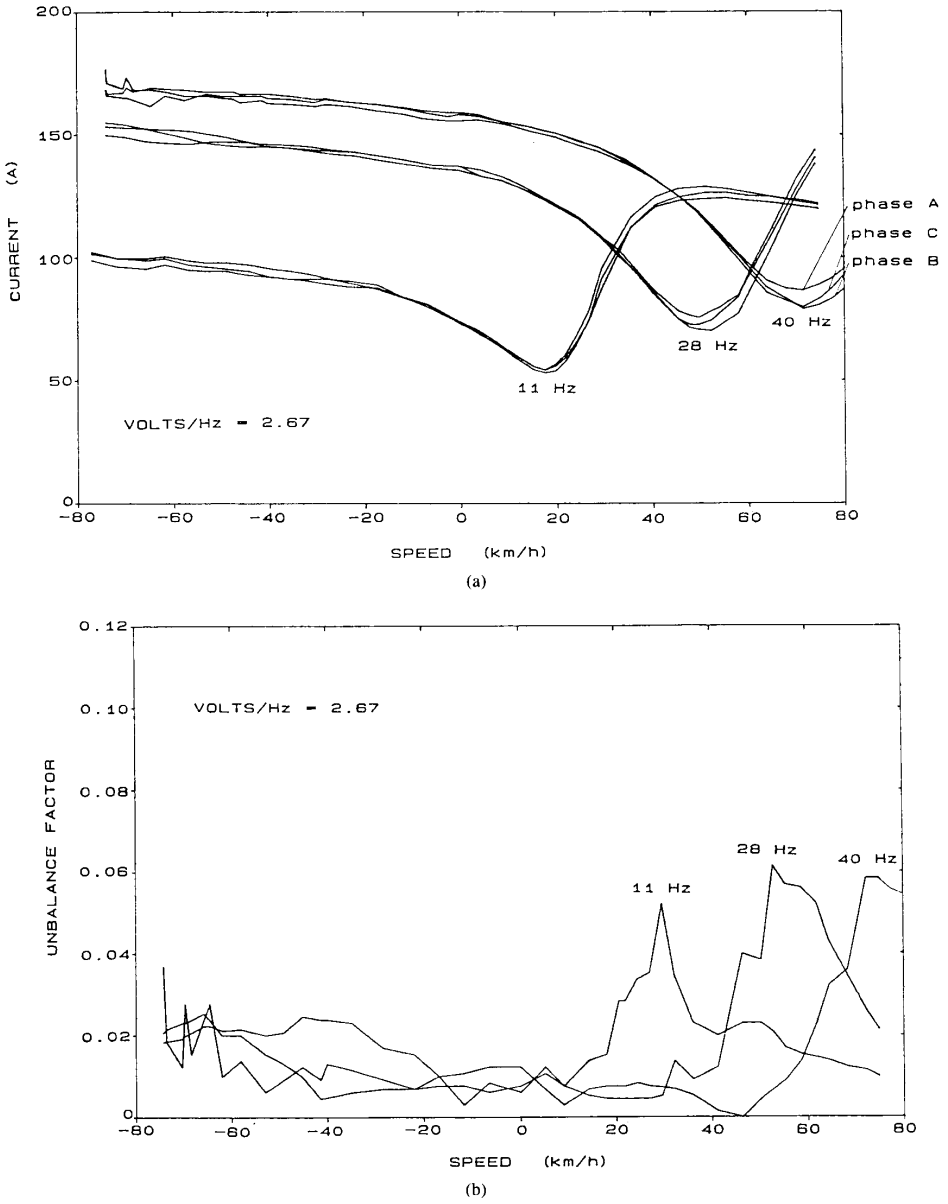

Fig. 3. Experimental results for the test LIM as a function of speed. (a) Phase currents. (b) Unbalance factor.

wheel to provide relative motion between rim-mounted guideway components (solid steel with an aluminum cap) and a stationary vehicle module (LIM). Design data for the LIM are given in Table I.

Constant voltage tests were performed at three frequencies—11, 28, and 40 Hz, with constant volts per hertz of 2.67. For analysis of phase unbalance, the individual phase currents were transformed using symmetrical components. An unbalance factor k_{unb} was defined as the ratio of the negative sequence current component to the positive sequence current component

$$k_{unb} = \left| \frac{I'}{I^+} \right|. \tag{29}$$

Fig. 3 shows the phase currents and the unbalance factor obtained by experiment. The computed results for the same conditions, as derived from the equivalent circuit

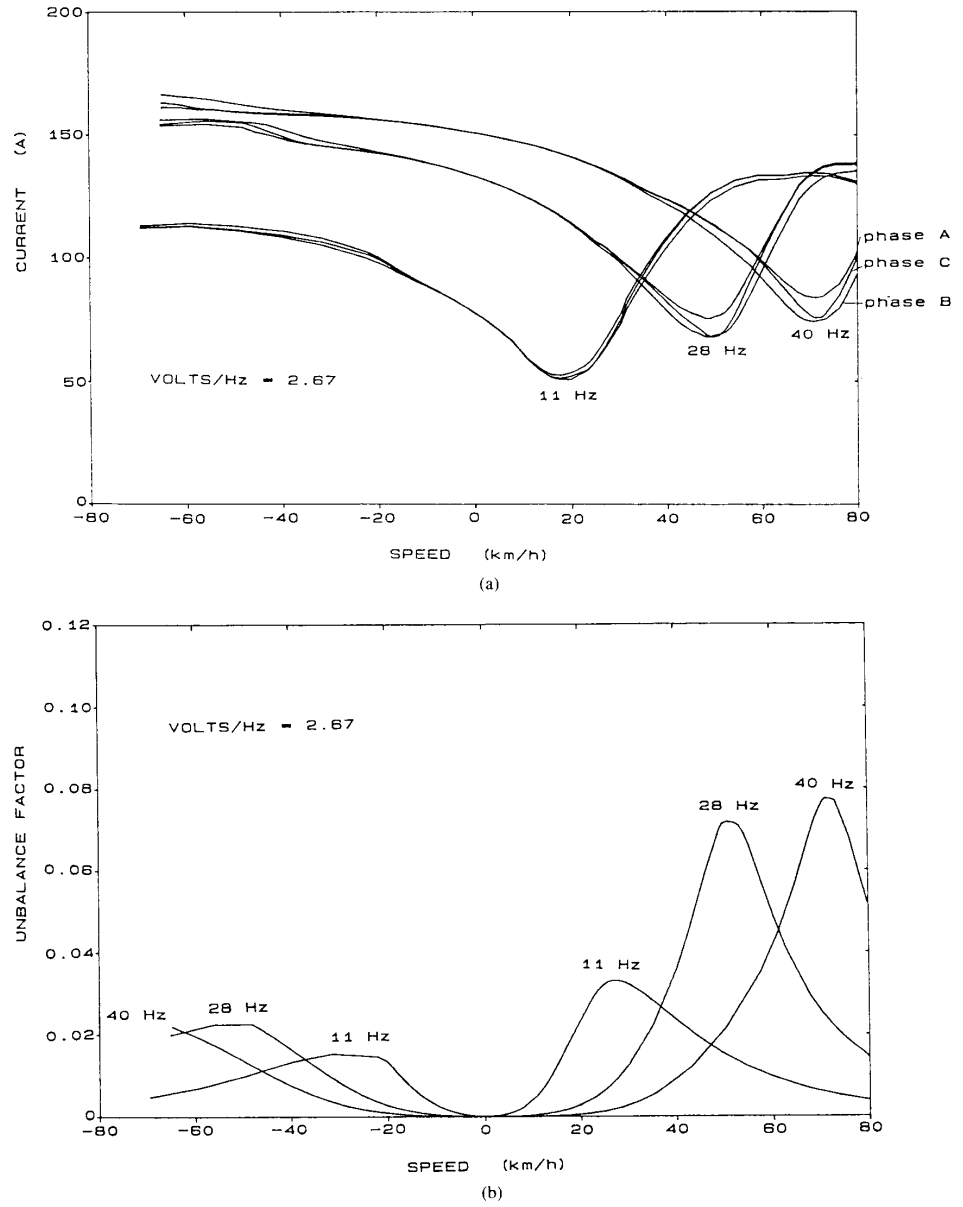

Fig. 4. Equivalent circuit results for the test LIM as a function of speed. (a) Phase currents. (b) Unbalance factor.

and finite-element analyses, are shown in Figs. 4 and 5, respectively.

The current follows the normal rotary induction machine pattern, remaining at a high value in the plugging and regenerative braking regimes and dropping to a minimum at synchronous speed. The minimum value, representing the magnetizing current, is high because of the large airgap of the LIM. Both sets of computed phase currents compare well with the experimental results.

At synchronous velocity, the highest current is in phase *A*, and the lowest current is in phase *B*. Both the experimental and computed results show the same trend. The current is highest in phase *A* because it is at the front end of the machine, and hence has a lower flux linkage and a low leakage reactance, due to the asymmetry in the flux distribution caused by end effect. By a similar reasoning, phase *C* being in the middle has a higher flux linkage and leakage reactance and hence a lower current, and phase *B*

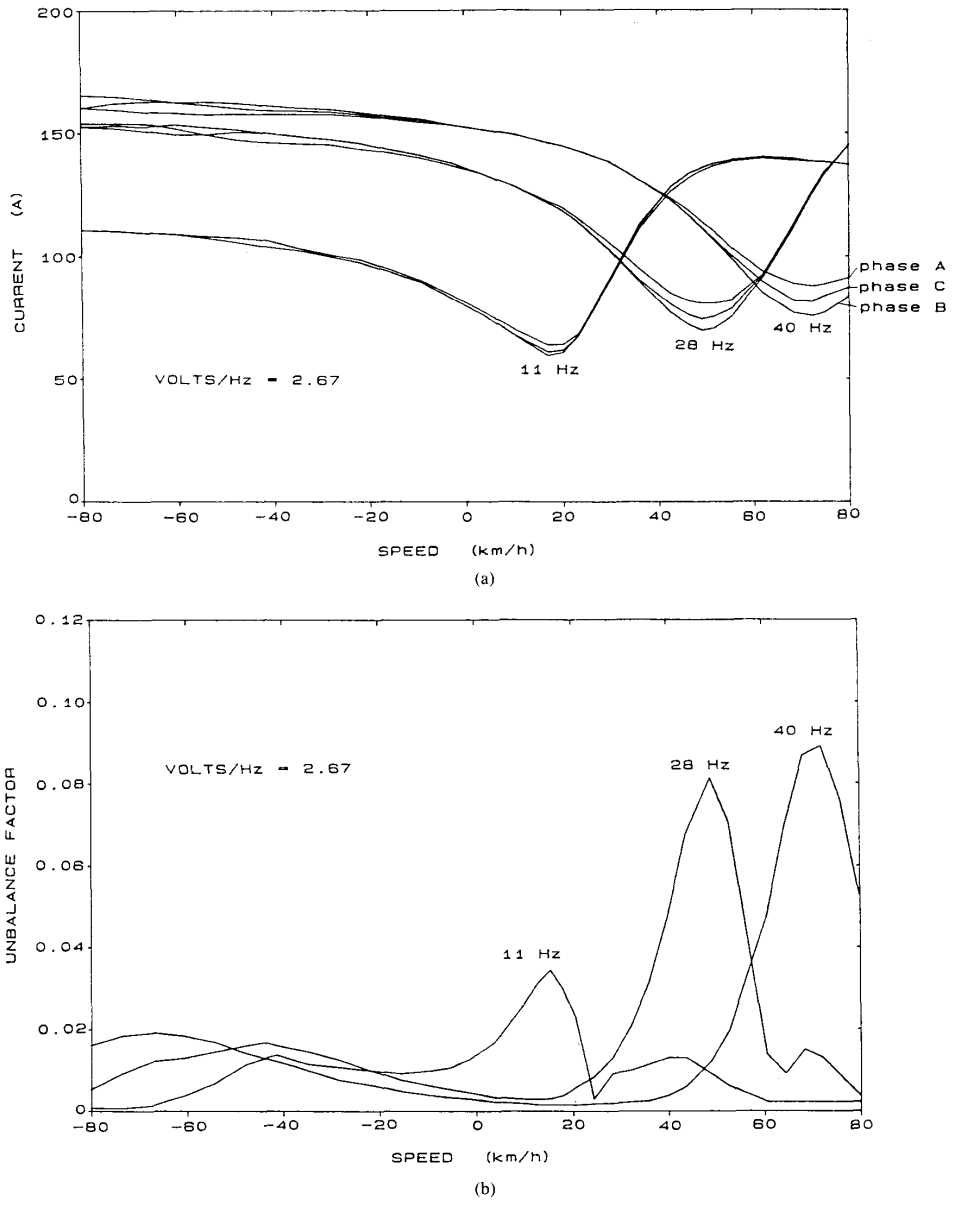

Fig. 5. Finite-element results for the test LIM as a function of speed. (a) Phase currents. (b) Unbalance factor.

being the furthest from the entry end of the machine has the highest flux linkage and leakage reactance and hence the lowest current.

Even though the computed and experimental unbalance factors show the same trend, differences in the amplitude and in the position of the peaks are evident. Experiments show that the maximum unbalance occurs at a speed slightly greater than synchronous speed. The results computed by the equivalent circuit agree with this, whereas the results computed by the finite-element method predict that the maximum phase unbalance is at synchronous speed. Phase unbalance, being mainly due to end effect, should be a maximum at synchronous speed according to theory by Yamamura [14]. The unbalance factor of synchronous speed should also increase with frequency, in accordance with the increasing end effect. The computed maximum unbalance factor increases more rapidly with frequency than observed experimentally.

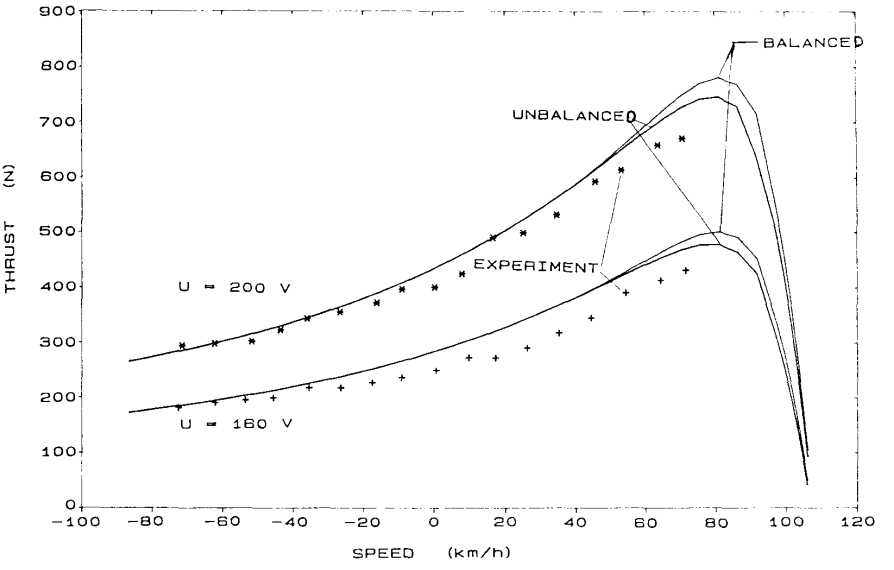

Fig. 6. Calculated and measured thrust-speed curves for the test LIM at 60 Hz.

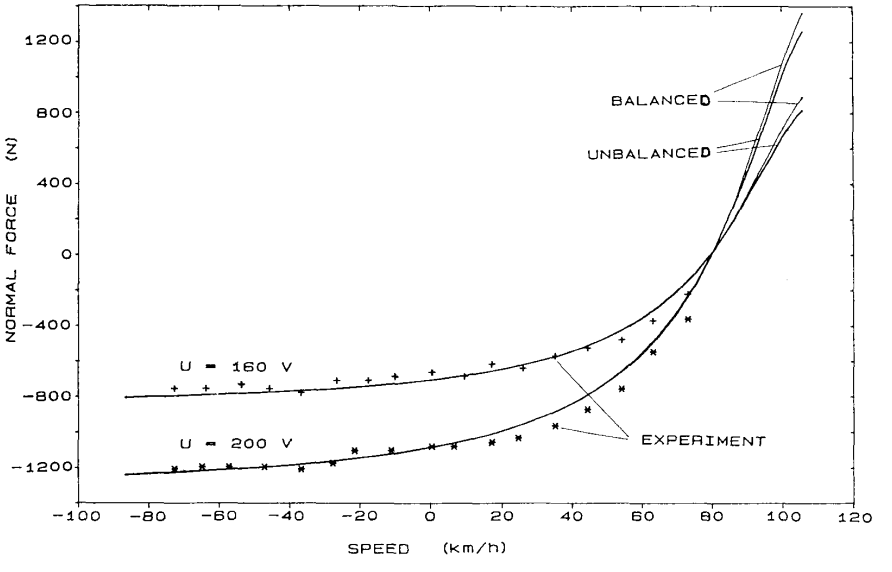

Fig. 7. Calculated and measured normal force for the test LIM at 60 Hz.

V. Effect of Phase Unbalance

The effect of unbalanced currents is to produce a backward-traveling field which degrades the performance characteristics of a LIM. The backward-traveling field produces braking thrust in the motoring region and forward thrust in the plugging region of operation.

Calculations from the equivalent circuit model and experimental values of the thrust and normal forces are presented in Figs. 6 and 7. Both calculated and experimental

TABLE II
Magnitude and Phase Angles of Phase Currents for Different Unbalance Factors
(Average current = 200 A)

k_{unb}	I_A	I_B	I_C
0.0	200 < 0	200 < −120	200 < 120
0.1	217.5 < 0	182.5 < −120.8	200 < 128.4
0.25	242 < 0	159 < −124.7	200 < 139.5
0.5	275 < 0	125 < −138.2	200 < 155.4

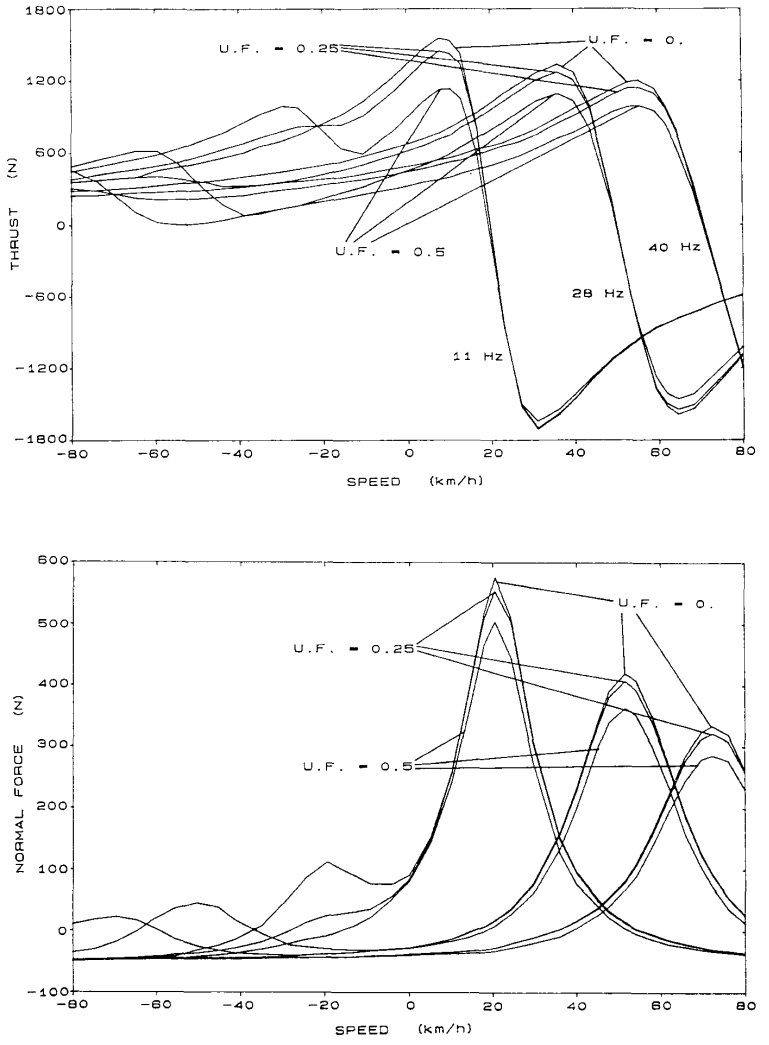

Fig. 8. Thrust and normal forces for the test LIM with unbalance factors of 0, 0.25, and 0.5.

results were obtained for constant voltage excitation of 160 and 200 V (line to line) at a frequency of 60 Hz. Phase unbalance has significant influence on thrust only near its maximum value, and maximum degradation is about 5 percent for the test LIM at 60 Hz. The normal force is less sensitive to phase unbalance and maximum influence occurs at synchronous speed.

To investigate the influence of higher unbalance factors on thrust, a finite-element analysis for constant current excitation was used. The current I_c was kept at 200 A, while both magnitude and phase of the currents I_A and I_B were chosen to give specific values of unbalance factor. Following the trend shown by previous experiments and computations I_A, I_B, and I_C were asssumed to have maximum, minimum, and average values, respectively. Table II shows the magnitude and phase angle of the phase currents for unbalance factors of 0.1, 0.25, and 0.5.

Fig. 8 shows the thrust and normal forces computed by the finite-element method for unbalance factors of 0, 0.25, and 0.5. The effect of phase unbalance can be seen to be very small for an unbalance factor of 0.25, but becomes significant for 0.5. In practice, unbalance factors above 0.25 are uncommon even for high-speed LIMs. The effect of unbalance is most significant in the plugging and regenerative regions.

To study the degradation of thrust with increase in phase unbalance, the peak thrust was computed for 6, 11, 28, and 40 Hz as a function of unbalance factor, as shown in Fig. 9. It is evident that the peak thrust is degraded more significantly at the lower frequencies.

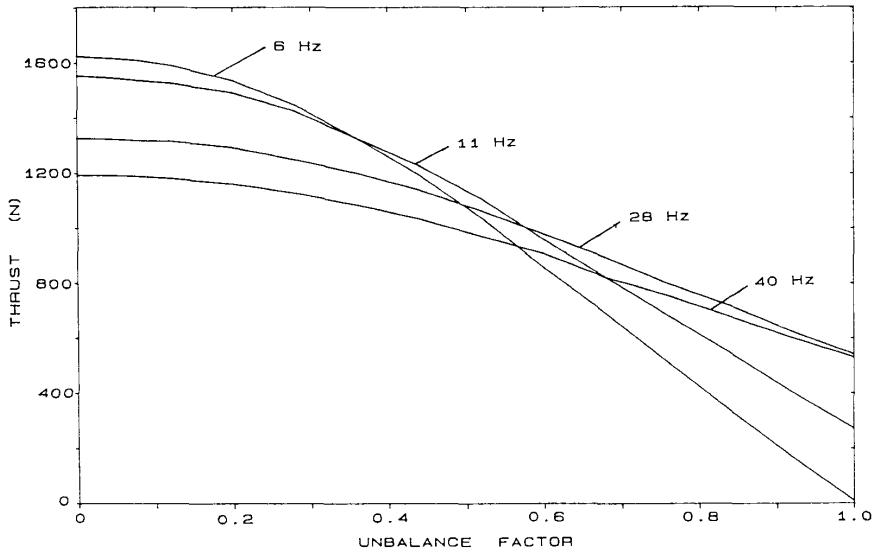

Fig. 9. Peak thrust for the test LIM as a function of unbalance factor.

VI. Conclusions

It has been shown that phase unbalance in a linear induction motor is associated with asymmetric primary windings and with the longitudinal end effect, both of which are a consequence of the finite length of the LIM. The longitudinal end effect is, however, the dominant factor.

Two methods for evaluating phase unbalance have been presented. The first is based on the development of a three-phase equivalent circuit of the LIM, which takes into account unbalanced phase currents. The basic (uncorrected) equivalent circuit parameters are determined from a computation of the two-dimensional field distribution in a uniformly wound LIM. Transverse edge effects are included by appropriate correction of the secondary conductivity [20]. The representation of the longitudinal end effect by phase-dependent end-effect factors, rather than by use of a Fourier series, makes it possible to determine unbalanced phase impedances while, at the same time, it provides some physical appreciation of the causes and consequences of unbalanced phase impedance.

The second method uses a modified form of the conventional finite-element technique, in which the phase currents as well as the nodal vector potentials are treated as unknowns.

It has been shown that phase unbalance is a function of speed and that it is maximum near synchronous velocity and a minimum at standstill. For low speed LIM's, e.g., for urban transit, the effect of phase unbalance on thrust and normal forces is rather small and for the test LIM is less than 5 percent. Moreover, the effect of phase unbalance is most significant at standstill and in the plugging region. Fortunately, while phase unbalance increases with velocity, the effect of phase unbalance on performance correspondingly decreases.

Appendix
Voltage Equations for Unequal-Phase Impedances

Under unbalanced conditions, the phase currents can be expressed by the following equations:

$$\begin{aligned} I_A &= I^+ + I^- \\ I_B &= a^2 I^+ + a I^- \\ I_C &= a I^+ + a^2 I^-. \end{aligned} \tag{30}$$

The currents I_A, I_B, I_C are in accordance with (2a) and (2b).

Including (14) and (15), the total phase voltages are then

$$\begin{aligned} V_A &= I_A Z_{pA} + I^+ Z_t^+ + I^- Z_t^- \\ V_B &= I_B Z_{pB} + a^2 I^+ Z_t^+ + a I^- Z_t^- \\ V_C &= I_C Z_{pC} + a I^+ Z_t^+ + a^2 I^- Z_t^-. \end{aligned} \tag{31}$$

Making use of (16a) and (16b), the expressions for the positive sequence and negative sequence voltages become

$$V^+ = \frac{I^+}{3}(Z_{p0} + 3Z_t^+) + \frac{I^-}{3} Z_p^- \tag{32}$$

$$V^- = \frac{I^-}{3}(Z_{p0} + 3Z_t^-) + \frac{I^+}{3} Z_p^+. \tag{33}$$

These expressions yield the positive and negative sequence currents (17a), (17b) and set up the equivalent circuit (Fig. 4) including current unbalance.

REFERENCES

[1] V. T. Chemerys and A. S. Pysmenny, "Electromagnetic field in the airgap of a linear induction machine under unbalanced excitation," (in Russian), *Prob. Electrodyn.*, vol. 32, pp. 33–43, 1972.

[2] R. Sankaran, K. P. P. Pillai, and K. A. Muraleedharan, "Voltage fed operation of linear induction motors under conditions of supply unbalance," *Proc. Inst. Elec. Eng.*, vol. 126, pp. 293–297, 1979.

[3] H. Yamazoe, "Analysis and experiments of single-sided linear induction motor," *Elec. Eng. in Japan*, vol. 100, pp. 9–18, 1980.

[4] C. Papageorgiou, "Linear induction motors under an unbalance three phase voltage," in *Proc. ICEM '80* (Athens, Greece, Sept. 1980), vol. 1, pp. 93–101.

[5] W. Deleroi, "Unbalanced terminal voltages and currents in the short primary linear induction motor," in *Proc. ICEM '80* (Athens, Greece, Sept. 1980), vol. 1, pp. 136–145.

[6] E. Gierczak, J. Fleszar, and J. Turowski, "Current asymmetry in the three phase linear motor," in *Proc. ICEM'82* (Budapest, Hungary, Sept. 1982), vol. 3, pp. 961–963.

[7] A. Bolopion, M. Poloujadoff, and R. D. Findlay, "Models for balanced voltage operation of linear induction motors," *IEEE Trans. Energy Conv.*, vol. EC-1, pp. 118–121, 1986.

[8] J. F. Gieras, A. R. Eastham, and G. E. Dawson, "Computation of the two-dimensional field in a single-sided linear induction motor fed with three-phase unbalanced current excitation," in *Proc. ICEM'86* (Munich, FRG, Sept. 1986), vol. 1, pp. 231–273.

[9] K. P. Kovacs, *Symmetrische Komponenten in Wechselstrommaschinen*. Basel, Switzerland: Birkhauser, 1962.

[10] N. N. Hancock, *Electric Power Utilization*. London, UK: Pitman & Sons Ltd., 1967.

[11] J. F. Gieras, A. R. Eastham, and G. E. Dawson, "Performance calculation for single-sided linear induction motors with a solid steel reaction plate under constant current excitation," *Proc. Inst. Elec. Eng.*, pt. B, vol. 132, pp. 185–199, 1985.

[12] ——, "The influence of secondary solid ferromagnetic plate thickness on the performance of single-sided linear induction motors," *Elec. Mach. Power Syst.*, vol. 10, pp. 67–77, 1985.

[13] J. F. Gieras, G. E. Dawson, and A. R. Eastham, "A new longitudinal end effect factor for linear induction motors," *IEEE Trans. Energy Conv.*, vol. EC-1, pp. 152–159, 1987.

[14] S. Yamamura, *Theory of Linear Induction Motors*. Tokyo, Japan: Univ. of Tokyo Press, 1972.

[15] J. F. Gieras, "Analytical method of calculating the electromagnetic field and power losses in ferromagnetic halfspace, taking into account saturation and hysteresis," *Proc. Inst. Elec. Eng.*, vol. 124, pp. 1098–1104, 1977.

[16] P. P. Silvester and R. L. Ferrari, *Finite Elements for Electrical Engineers*. Cambridge, UK: Cambridge Univ. Press, 1983.

[17] P. G. Potter and G. K. Cambrell, "A combined finite element and loop analysis for nonlinearly interacting magnetic field and circuit," *IEEE Trans. Magn.*, vol. MAG-19, pp. 2352–2355, 1983.

[18] D. Shen, G. Meunier, J. L. Coulomb, and J. C. Sabonnadiere, "Solution of magnetic fields and electrical circuits combined problems," *IEEE Trans. Magn.*, vol. MAG-21, pp. 2288–2291, 1985.

[19] T. Nakata and N. Takahashi, "Direct finite element analysis of flux and current distributions under specified conditions," *IEEE Trans. Magn.*, vol. MAG-18, pp. 325–330, 1982.

[20] R. L. Russell and K. H. Norsworthy, "Eddy currents and wall losses in screened-rotor induction motors," *Proc. Inst. Elec. Eng.*, vol. 105A, pp. 163–175, 1958.

[21] G. E. Dawson and A. R. Eastham, "The comparative performance of single-sided linear induction motors with squirrel-cage, solid-steel, and aluminum-capped reaction rail," in *Proc. 16th Annu. IEEE IAS Meet.*, (Philadelphia, PA, Oct. 1981), IEEE Conf. Rec. 81CH1678-2, pp. 323–329.

K. Adamiak received the M.Sc. and Ph.D. degrees in electrical engineering from the Technical University of Szczecin, Szczecin, Poland, and the D.Sc. degree from the Technical University of Gdańsk, Gdańsk, Poland, in 1974, 1976, and 1983, respectively.

His research activities include electromagnetic field analysis in electric machines and other electromagnetic devices. He is an Associate Professor in the Department of Electrical Engineering, Technical University of Kielce, Kielce, Poland. He is the author of numerous scientific papers and holds a Polish patent. At present, he is a Visiting Professor at Queen's University, Kingston, Ont., Canada.

Krishnamoorthy Ananthasivam was born in South India, on April 10, 1961. He received the B.Tech. degree in electrical engineering from the Indian Institute of Technology, Madras, India, in 1983, and the M.Sc. (Eng.) degree in electrical engineering from Queen's University, Kingston, Ont., Canada, in 1985.

His current interests are in the area of software development for engineering applications, and he is currently employed as a Software Engineer in South India.

Graham E. Dawson (S'66–M'69) was born in North Vancouver, BC, Canada, on November 11, 1939. He received the B.A.Sc., M.A.Sc., and Ph.D. degree from the University of British Columbia, Vancouver, in 1963, 1966, and 1970, respectively.

In 1969 he joined the Department of Electrical Engineering, Queen's University, Kingston, Ont., Canada, as an Assistant Professor. He was promoted to Associate Professor in 1975 and to Professor in 1981. His electrical engineering research activities have been associated with the transportation industry where he has current interest in the design and performance of rotary and linear traction motors and energy management of transportation systems.

Dr. Dawson is a Registered Professional Engineer in the Province of Ontario and a member of the Canadian Society for Electrical Engineering.

Anthony R. Eastham (M'75–SM'83) received the B.Sc. degree in physics from the University of London, London, UK, in 1965, and the Ph.D. degrees from the University of Surrey, UK, in 1969.

After research work at Plessey Telecommunications Ltd. and at the University of Warwick, he joined the Canadian Institute of Guided Ground Transport where he coordinated a group that technically defined, component tested, and assessed high-speed Maglev in Canada. He is now a Professor of Electrical Engineering at Queen's University, Kingston, Ont., Canada, having joined the faculty in 1978. His research activities include innovative urban and high-speed transportation, linear electric drives, and electromagnetic analysis.

Dr. Eastham is a Registered Professional Engineer of the Province of Ontario.

Jacek F. Gieras (M'83) was born in [redacted] on [redacted]. He received the M.Sc. (Mgr inż.) degree in electrical engineering from the Technical University of Łódź, and the Ph.D. (Dr inż.) and D.Sc. (Dr hab.) degrees from the Technical University of Poznań, Poznań, Poland, in 1971, 1975, and 1980, respectively.

His research activities include analysis of electromagnetic fields in electrical machines and devices, computer-aided design of electrical machines, magnetic levitation, and industrial drives. At present, he is a Visiting Associate Professor at Queen's Univeristy, Kingston, Ont. He is the co-author of a monograph *Induction Machines with Solid Rotor* published by the Polish Scientific Publishing House (Warszawa-Poznań, Poland) in 1977, author of a textbook *Special Purpose Electric Machines* (ATR Bydgoszcz, Poland, 1983), and author of 65 scientific papers published in Poland, Great Britain, USA, India, FRG, East Germany, Switzerland, Czechoslovakia, and Hungary. He holds four Polish patents.